J Shoulder Elbow Surg (2019) 28, 1166–1174

ELSEVIER

Journal of Shoulder and Elbow Surgery

www.elsevier.com/locate/ymse

Biomechanical comparison of 2 augmented glenoid designs: an integrated kinematic finite element analysis

Vani J. Sabesan, MD[a,*], Diego J.L. Lima, MD[a], James D. Whaley, MD[b], Varun Pathak, MS[c], Liying Zhang, PhD[c]

[a]*Department of Orthopedic Surgery, Cleveland Clinic Florida, Weston, FL, USA*
[b]*Department of Orthopedic Surgery, Beaumont Health System, Royal Oak, MI, USA*
[c]*Department of Biomedical Engineering, Wayne State University School of Medicine, Detroit, MI, USA*

Background: Augmented glenoid implants are available to help restore the biomechanics of the glenohumeral joint with excessive retroversion. It is imperative to understand their behavior to make a knowledgeable preoperative decision. Therefore, our goal was to identify an optimal augmented glenoid design based on finite element analysis (FEA) under maximum physiological loading.

Methods: FEA models of 2 augmented glenoid designs—wedge and step—were created per the manufacturers' specifications and virtually implanted in a scapula model to correct 20° of retroversion. Simulation of shoulder abduction was performed using the FEA shoulder model. The glenohumeral force ratio, relative micromotion, and stress levels on the cement mantle, glenoid vault, and backside of the implants were compared between the 2 designs.

Results: The force ratio was 0.56 for the wedge design and 0.87 for the step design. Micromotion (combination of distraction, translation, and compression) was greater for the step design than the wedge design. Distraction measured 0.05 mm for the wedge design and 0.14 mm for the step component. Both implants showed a similar pattern for translation; however, compression was almost 3 times greater for the step component. Both implants showed high stress levels on the cement mantle. At the glenoid vault and on the implants, the stress levels were 1.65 MPa and 6.62 MPa, respectively, for the wedge design and 3.78 MPa and 13.25 MPa, respectively, for the step design.

Conclusion: Implant design slightly affects joint stability; however, it plays a major role regarding long-term survival. Overall, the augmented wedge design provides better implant fixation and stress profiles with less micromotion.

Level of evidence: Basic Science Study; Computer Modeling

Keywords: Augmented glenoid; finite element analysis; step design; wedge design; total shoulder arthroplasty; glenoid bone loss; glenoid retroversion

This study was institutional review board exempt because of the absence of either animal or human subjects studied.

*Reprint requests: Vani J. Sabesan, MD, Department of Orthopedic Surgery, Cleveland Clinic Florida, 2950 Cleveland Clinic Blvd, Weston, FL 33331, USA.

E-mail address: sabesav@ccf.org (V.J. Sabesan).

Total shoulder arthroplasty (TSA) has proved to be successful in providing pain relief and restoring range of motion in patients with glenohumeral osteoarthritis (OA).[3,19] Excessive acquired glenoid retroversion develops in patients with

1058-2746/$ - see front matter © 2019 Published by Elsevier Inc. on behalf of Journal of Shoulder and Elbow Surgery Board of Trustees.
https://doi.org/10.1016/j.jse.2018.11.055

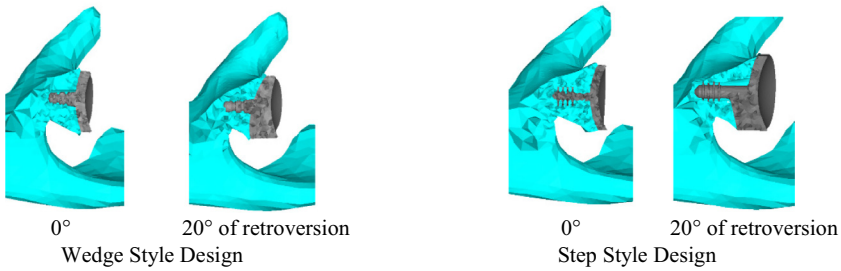

Figure 1 Horizontal sections through center of glenoid implant of finite element analysis models showing simulated 0° and 20° retroverted scapulae with implanted standard and augmented glenoids: 0° and 20° of retroversion for wedge-style design (*left*) and 0° and 20° of retroversion for step-style design (*right*).

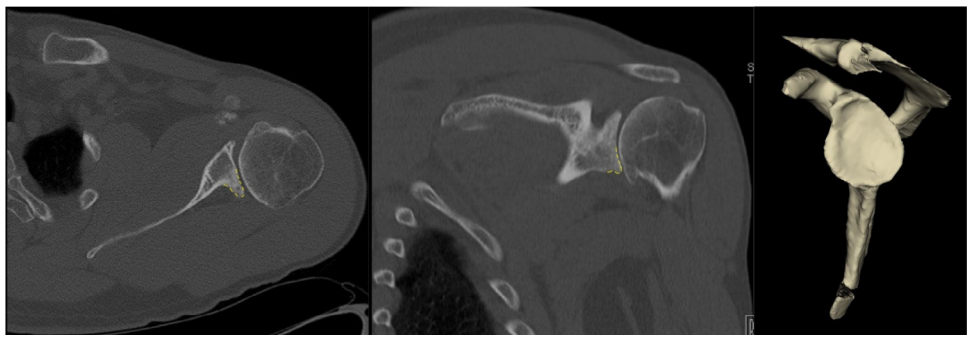

Figure 2 Average type B2 glenoid based on Walch classification showing bone loss in posteroinferior quadrant.

posterior bone loss due to advanced OA, which has been classified as a Walch type B2 and, more recently, type B3 glenoid bone loss pattern.[6,18,24] This excessive retroversion is challenging to manage with asymmetrical reaming and standard glenoid components.[1,6,8,10,18,24,27,28] Glenoid bone loss leads to fixation stresses and eccentric loading and, consequently, an increased risk of glenoid implant loosening, which is the most common reason for revision surgery.[5,6,8,12-15,18,20,25,30] Other treatment options for the management of type B2 erosions are reverse TSA, structural glenoid bone grafting, and augmented glenoid components. However, none has shown clinical superiority.[4,6]

The use of augmented glenoid components is becoming more popular among shoulder specialists to account for moderate to severe posterior glenoid bone loss.[26] These implants are typically designed with a posteriorly oriented step or wedge, which assumes that the maximum glenoid erosion is oriented perpendicular to the implant's superior-inferior axis (Fig. 1). The benefit of this augmented glenoid implant option is removal of less bone and correction of deformity resulting in less humeral medialization and muscle shortening.[18] Thus, in theory, augmented glenoid components reduce posterior loading and shear stresses at the implant interface, thereby improving implant stability.[26] Although these implants are intended to conserve subarticular bone, it has been suggested that type B2 bone loss is not oriented purely in the posterior direction. Recent literature has shown that the average type B2 glenoid has bone loss in the posteroinferior quadrant directed toward the 8-o'clock position (right shoulder) (Fig. 2).[1,4] Consequently, this may result in increased bone removal in the posterosuperior quadrant or possibly malrotation of components to facilitate full backside seating.

Unfortunately, there is limited literature on the performance of augmented glenoids. Finite element analysis (FEA) has been widely used in the past 2 decades to address various questions regarding shoulder arthroplasty.[16] Recent FEA studies of glenoid components have shown less bone removal but higher peak stresses with augmented glenoids than with standard implants for correction of arthritic glenoids in a static setting.[1,6,9] Although static testing has been reported, more physiological loading conditions would better simulate the clinical performance of these augmented glenoid implants. It also has been reported that the largest load observed on the glenohumeral joint occurs during abduction.[9,11] Therefore, the purpose of this study was to assess the biomechanical differences between 2 augmented glenoid implant designs in TSA under maximum clinically relevant physiological loading over time through a new integrated finite element model for dynamic analyses.

Materials and methods

This biomechanical study consisted of testing 2 different augmented glenoid designs (wedge and step) under physiological loading conditions using an integrated FEA shoulder model for dynamic analysis. Specifically, the highest-loading potential scenario was tested by putting the shoulder through a range of motion (0°-90° of abduction) (Fig. 3) that has been shown to create the highest joint

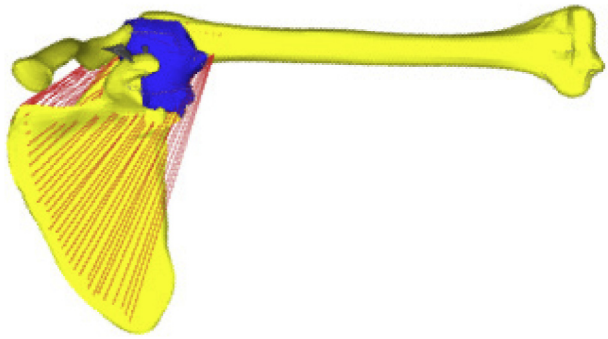

Figure 3 Finite element model of glenohumeral joint, with accurate representation of rotator cuff origin and insertion, simulating 90° of glenohumeral abduction.

reaction forces in the glenohumeral joint.[11] We also evaluated the optimal implant design based on mechanical parameters related to loosening and fixation failure. The conformity of the 2 different prosthetic joints was standardized at 6 mm of radial mismatch.

Glenoid components and FEA model generation

The 2 augmented glenoid component designs modeled were an all-polyethylene, peg, curved-back, step design (Global StepTech; DePuy, Warsaw, IN, USA) and an all-polyethylene, wedge glenoid design (Equinoxe; Exactech, Gainesville, FL, USA). The computer-aided design models of implant components were provided by the manufacturers. The finite element models of the implants were meshed with 1-mm element resolution using HyperMesh (Altair Engineering, Troy, MI, USA), ICEM-CFD (ANSYS, Canonsburg, PA, USA), and ANSA (BETA CAE Systems, Root, Switzerland) (Fig. 4). The material of the glenoid implant was modeled as linearly elastic, isotropic, homogeneous material of high molecular weight (polyethylene with a Young modulus of 1.2 GPa and Poisson ratio of 0.46). The polymethyl methacrylate bone cement material was defined as an elastic model with a Young modulus and Poisson ratio of 2.0 GPa and 0.23, respectively. A rigid humeral head model was used based on manufacturer design defined as rigid cobalt-chromium alloy (Tables I and II). The glenoid bone model was considered linear elastic material, with nonhomogeneous properties related to its density simulating both cortical and cancellous properties.[17]

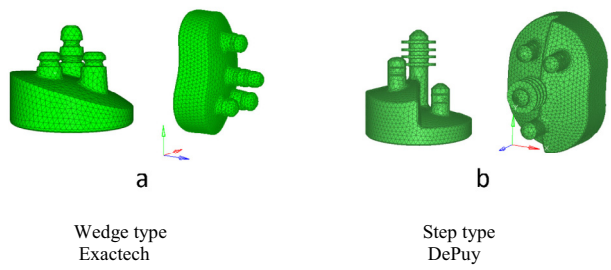

Figure 4 Finite element models of augmented wedge and step glenoid component designs: wedge-type Exactech design **(a)** and step-type DePuy design **(b)**.

Table I Material properties defined for FEA wedge model

Component type	Material model	Property
Humeral head implant	Elastic	$\rho = 7.90 \times 10^{-6}$ kg/mm^3 E = 210 GPa $\nu = 0.3$
Glenoid implant (polyethylene)	Piecewise elastic	$\rho = 1.00 \times 10^{-6}$ kg/mm^3 E = 1.26 GPa $\nu = 0.46$ Yield strength = 0.021 GPa
Cement (PMMA)	Piecewise elastic	$\rho = 1.00 \times 10^{-6}$ kg/mm^3 E = 2 GPa $\nu = 0.23$
Mounting block (polyurethane)	Foam	$\rho = 3.20 \times 10^{-7}$ kg/mm^3 E = 0.193 GPa

FEA, finite element analysis; *ρ*, rho, defines the density of the material kg/mm^3, kilograms per 1 cubic millimeter; *E*, the Young's modules that defines material's stiffness; *GP*, gigapascals; *ν*, nu, defines Poisson's ration; *PMMA*, polymethyl methacrylate.

Table II Material properties defined for FEA step model

Component type	Material model	Property
Humeral head implant	Elastic	$\rho = 7.90 \times 10^{-6}$ kg/mm^3 E = 210 GPa $\nu = 0.3$
Glenoid implant (polyethylene)	Piecewise elastic	$\rho = 1.00 \times 10^{-6}$ kg/mm^3 E = 0.52 GPa $\nu = 0.46$ Tangential modulus = 0.1 GPa Yield strength = 0.012 GPa
Cement (PMMA)	Piecewise elastic	$\rho = 1.00 \times 10^{-6}$ kg/mm^3 E = 2 GPa $\nu = 0.23$
Mounting block (polyurethane)	Foam	$\rho = 3.20 \times 10^{-7}$ kg/mm^3 E = 0.193

FEA, finite element analysis; *ρ*, rho, defines the density of the material kg/mm^3, kilograms per 1 cubic millimeter; *E*, the Young's modules that defines material's stiffness; *GP*, gigapascals; *ν*, nu, defines Poisson's ration; *PMMA*, polymethyl methacrylate.

FEA model ASTM simulation testing for validation

A standard ASTM test that evaluates glenoid loosening or dissociation (F2028-08) from humeral head translation in an anterior-posterior direction was used to validate our model (Fig. 5, *a*). To investigate the mechanical effect of different augmented implant designs on the scapular bone, FEA models of the scapular bone were developed and integrated with the glenoid models. The geometry of the scapula of the shoulder was taken from the Global Human Body Models Consortium (GHBMC, Troy, MI, USA) 50th percentile male human body model developed and validated for dynamic analysis.[21] This scapula model was based on computer-aided design data obtained from the computed tomography and magnetic resonance imaging scans of a 50th percentile male subject. The FEA scapular bone mesh was modified to simulate a 20° retroverted

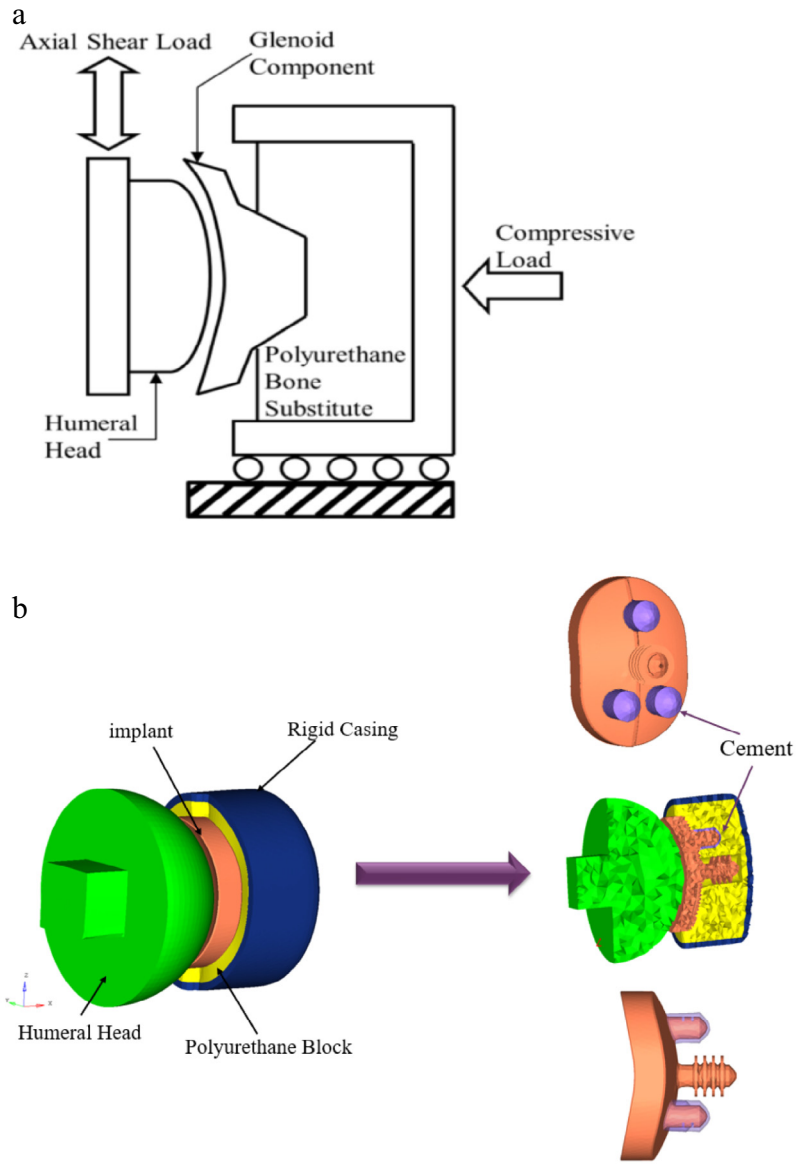

Figure 5 **(a)** Schema of ASTM subluxation test. **(b)** Finite element analysis model setup for ASTM subluxation test simulation. The contact interface was defined between the back of the glenoid implant and the bone substitute.

shoulder, and the appropriate augmented implant designs were fitted to the respective scapula model to simulate desired retroversion correction (+7 mm for the step-style design and 16° for the wedge-style design). The glenohumeral joints were then modeled, and all associated capsular ligaments and muscles with their proper locations of origin and insertion based on the atlas were meshed to simulate complete shoulder kinematics (Fig. 6).

The cement elements were generated between the bone and implant at the proper site per the manufacturer's specification. The implant-cement-bone interfaces were bonded directly via nodal connectivity (Fig. 7). Cement was placed over the pegs of the implant based on the manufacturer's instructions specified for the type of glenoid model. The cement was directly connected to the polyurethane block and the implant peg (Fig. 5, *b*).

Abduction simulation

A dynamic, nonlinear FEA solver (LS-Dyna, San Francisco, CA, USA) was used to simulate abduction from 0°-90°. An axial load of 750 N was applied perpendicular to the glenoid implant, humeral head translation occurred along the true anterior-posterior direction of the glenoid, and shear movement at 25 mm/s was applied in the parallel direction of the glenoid by the humeral head to recreate edge loading.[19] The rest of the direction was constrained, and no rotation was allowed (Fig. 8). The translation of the humeral head was simulated based on the loading used in the ASTM test to investigate the biomechanical responses of the bone and compare the 2 different augmented designs. Each implant underwent 50,000 cycles at a constant frequency of 2 Hz. This cyclic loading represents

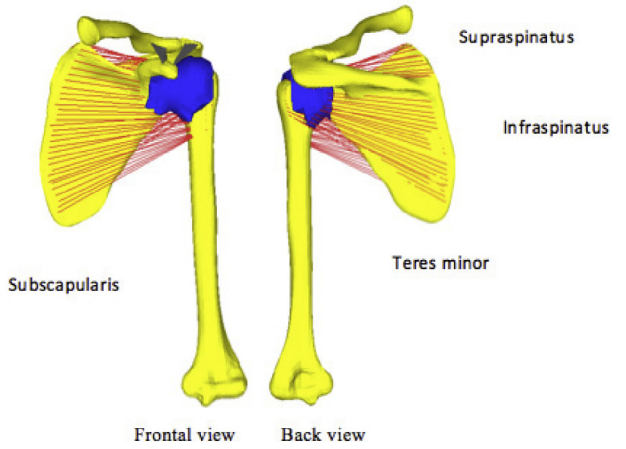

Figure 6 Anterior and posterior views of total shoulder arthroplasty finite element model with rotator cuff muscles in left shoulder.

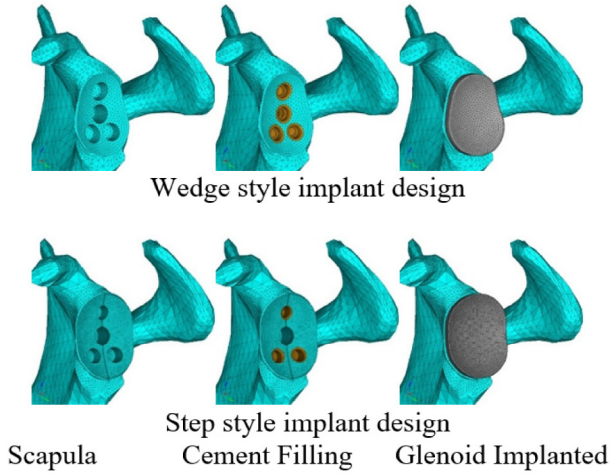

Figure 7 Finite element analysis models of scapula, cement, and implanted glenoid for both implant designs.

approximately 25 high-load activities per day (eg, getting out of a chair or lifting a suitcase) for 5 years.[19]

The glenohumeral subluxation force, glenoid micromotion (compression, distraction, and translation), and stress levels were outputs evaluated in the FEA model and compared between the 2 designs to evaluate the effect of physiological abduction range of motion on the glenohumeral joint. Furthermore, validation of the FEA models for both designs was achieved through direct comparison with the results from the ASTM tests by Anglin et al[2] and Sabesan et al[19] to ensure the accuracy of the mechanical responses as predicted by the FEA models.

Outcome variables

Model-predicted biomechanical responses including glenohumeral contact force, implant von Mises stress, underlying bone and cement mantle stresses, and micromotion at the bone-cement interface were assessed and compared between the 2 segmented designs.

Results

Force ratio

The shear force required to assess instability was expressed as a ratio of the applied compressive force and defined as the force ratio.[7] The model prediction of the force ratio was 0.56 for the augmented wedge design and 0.87 for the augmented step design. The step design had a higher force ratio than the wedge design at similar conformity settings (Table III).

Micromotion

Micromotion was defined as a combination of 3 components based on different directions (axes) (Fig. 9). Distraction measured 0.05 mm for the wedge design compared with 0.14 mm for the step component. Both implants showed a similar pattern with anterior-to-posterior translation at 0.005 mm for the augmented wedge design and 0.007 mm for the step design. The greatest difference between augmented glenoid components was seen in compression, where the step component showed almost 3 times more micromotion than the wedge implant design. Overall, the step design registered greater micromotion than the wedge design during abduction ROM (Table IV).

Table III Shearing force required to instigate humeral instability

Implant design	Force ratio
Wedge*,†	0.56
Step*,‡	0.87

* Six-millimeter radial mismatch between humeral head and glenoid prosthetic components.
† Sixteen-degree backside full wedge.
‡ Seven-millimeter backside step.

Table IV Measurements of micromotion during FEA model biomechanical testing

Implant design	Micromotion, mm		
	Distraction*	Translation†	Compression‡
Wedge§,‖	0.05	0.005	0.06
Step§,¶	0.14	0.007	0.16

FEA, finite element analysis.
* Micromotion away from bone substitute, within x-axis.
† Micromotion within superior-inferior axis parallel to glenoid plane.
‡ Micromotion toward bone substitute, within x-axis.
§ Six-millimeter radial mismatch between humeral head and glenoid prosthetic components.
‖ Sixteen-degree backside full wedge.
¶ Seven-millimeter backside step.

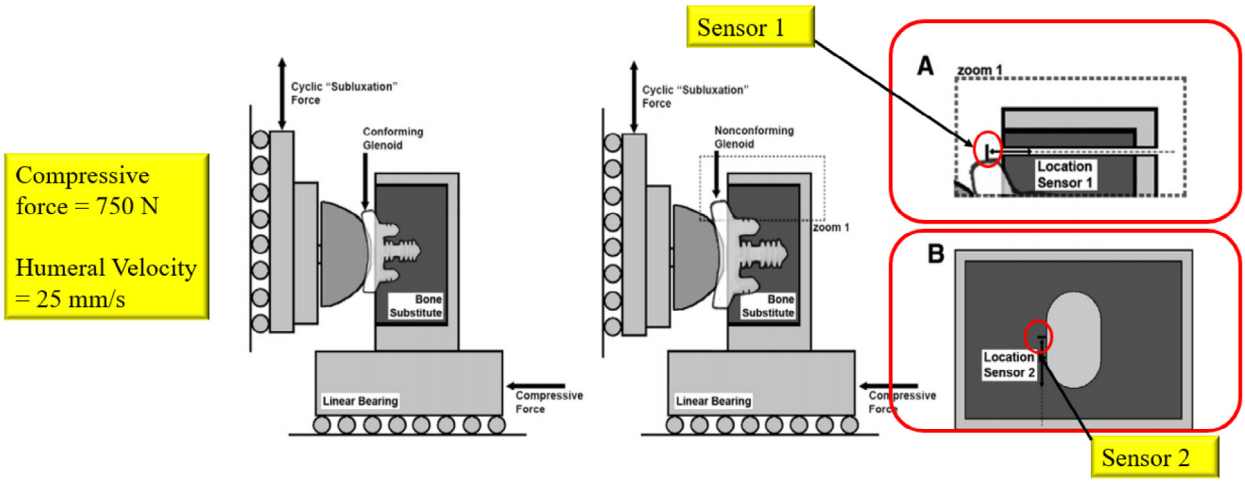

Figure 8 Location of sensors to predict mechanical response of implant and bone during anterior-posterior direction for finite element simulation. **(A)** One differential variable reluctance transducer sensor was fitted at the superior pole of the glenoid, as recommended by ASTM standards to measure glenoid distraction and compression. **(B)** The second sensor was fitted on the lateral side of the glenoid parallel to the axis of actuator motion for the measurement of anterior-posterior glenoid translation.

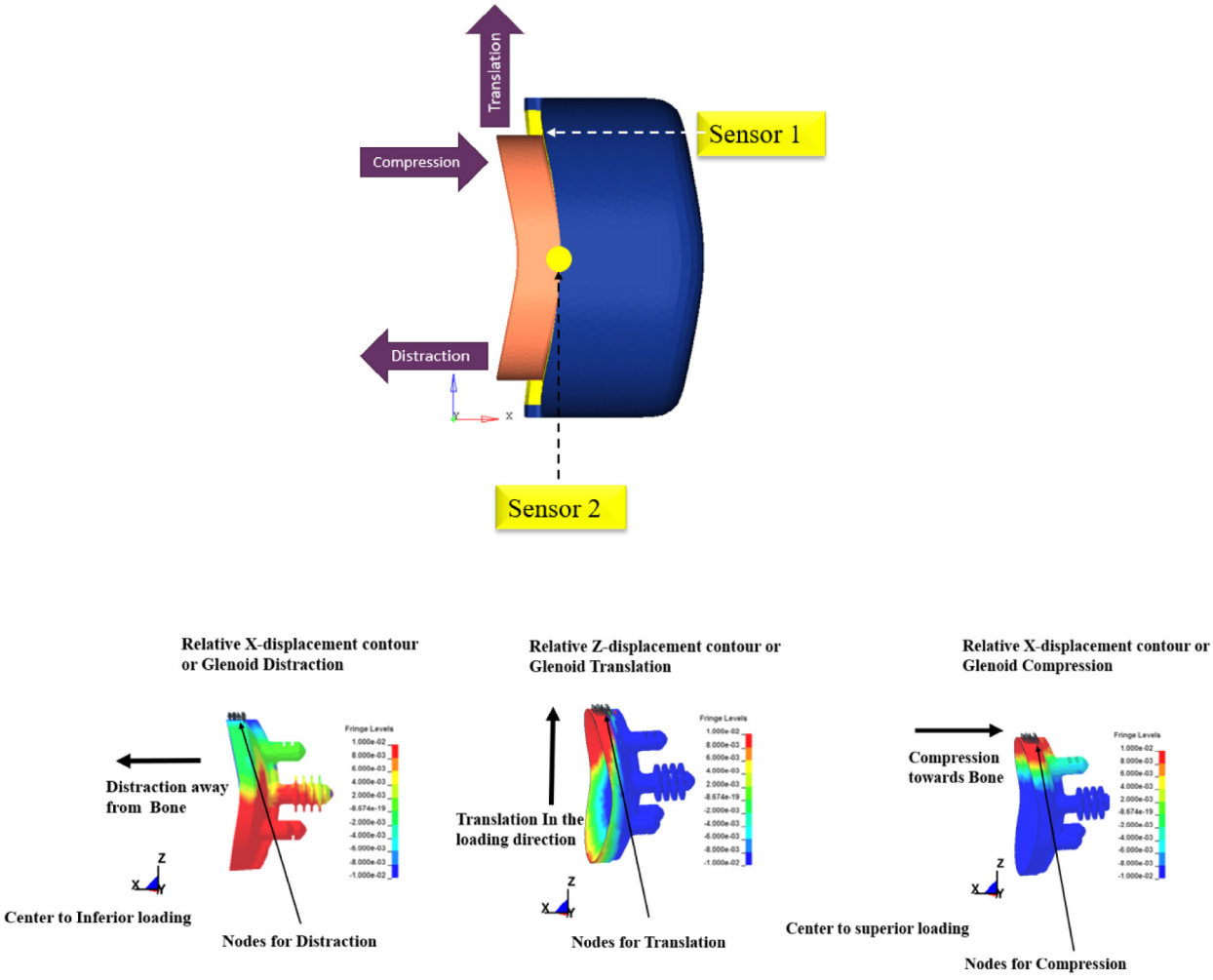

Figure 9 Micromotion resolved into 3 movements: distraction, translation, and compression relative to fixed scapular bone substitute.

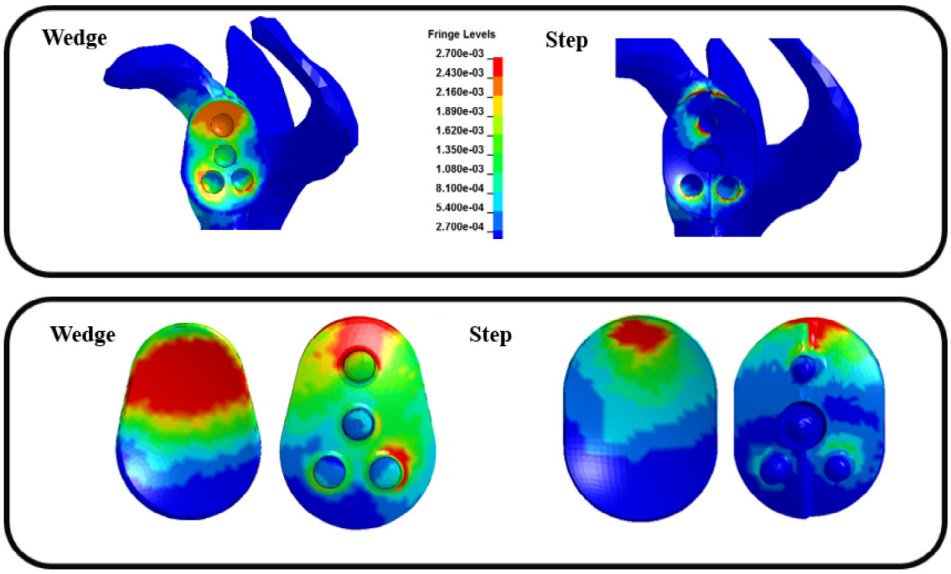

Figure 10 Von Mises stress distribution in scapular bone and on implant frontal side and backside.

Glenoid vault stress levels

The location of the stress pattern varied between different augmented designs. The level of stress generated during abduction on the glenoid vault was 1.65 MPa for the wedge design and 3.78 MPa for the step design. All stress levels were found to be below the determined bone failure limit (10-20 MPa).

Glenoid component stress levels

The results for implant shear stress measured on the backside of the wedge and step components were 6.62 MPa and 13.25 MPa, respectively. However, all of these polyethylene stress levels were below the threshold reported for polyethylene damage, which is approximately 20 MPa.[6] Figure 10 shows the stress distribution patterns and localization in the scapular bone and glenoid implant with the wedge and step augmented designs used. High stress was localized at the bone around the peg and extended to the bone-implant interface at the back of the implant.

Cement stress levels

Both components showed high levels of stress measured on the cement mantle, which exceeded the endurance limit for cement fracture (4 MPa after 1 million loading cycles).[28] Cement stress levels measured 6.4 MPa and 4.6 MPa for the wedge and step designs, respectively. All von Mises stress levels are shown in Table V.

Table V Measurements of backside implant stress during FEA model biomechanical testing

Implant design	von Mises stress level, MPa		
	Vault of glenoid bone	Implant backside	Cement mantle
Wedge*,†	1.65	6.62	6.4
Step*,‡	3.78	13.25	4.6

FEA, finite element analysis.
* Six-millimeter radial mismatch between humeral head and glenoid prosthetic components.
† Sixteen-degree backside full wedge.
‡ Seven-millimeter backside step.

Discussion

Posterior glenoid bone loss in patients with glenohumeral OA is an important issue to be corrected when performing a TSA. Placement of the glenoid in excessive retroversion leads to eccentric glenoid loading and early implant loosening. Studies have shown a high degree of success in correction of posterior glenoid wear combining different approaches including the use of augmented glenoid components.[6] The outcomes of these augmented glenoid components, however, have not been well described. We used an integrated FEA kinematic model to evaluate the optimal augmented glenoid design for 2 commercially available augmented glenoid components, wedge versus step, to predict failure patterns over time during maximum physiological loading simulated with shoulder abduction. Our results suggest that the wedge glenoid design may have a better performance and fixation profile with physiological loading; however, further clinical research is needed to verify these biomechanical results.[2]

In terms of stability and fixation stresses, we found that the wedge design provided less joint stability (36% less) than the step design. Although comparable data are currently unavailable in the literature, it has been shown that the force ratio or stability changes with increased loads owing to polyethylene deformation and rigidity of the implant material.[7] Our stability results appeared to be influenced by the material stiffness, which was 2 times higher for the wedge glenoid compared with the step glenoid. In addition to joint stability, the high cement mantle stresses seen for both augmented glenoid designs were concerning. The cement mantle is a critical interface for early fixation between the implant and bone, and it is often the site of failure leading to aseptic loosening. Radiolucent lines at the cement-bone interface are thought to be predictive markers of impending component loosening and are still frequently observed.[1] Although previous results reported decreased cement interface stresses and increased bone fatigue life when a posterior wedge glenoid component was implanted,[1,6] our results showed that cement mantle stresses of both augmented designs were above the endurance limit for cement mantle fracturing. These results may urge further research for alternative early-fixation options and designs.

Nonetheless, the step design predominantly presented at least 2 times higher levels of stress when the glenoid vault and the backside of the implants were evaluated. Even though, in our model, it was not enough to surpass the bone and implant failure limit, it seems that a step design represents a higher risk of implant failure over time because of an increased risk of bone and implant fatigue or fracture.[29] Such a response may be related to the abrupt geometrical alteration of the step design as opposed to the progressive augmentation of the posterior aspect of the wedge implant.

In terms of the optimal design for implant fixation, our study results showed that the amount of micromotion was higher for the step design. Specifically, distraction and compression were 3 times greater for the augmented step design than for the wedge design based on our FEA. These small changes in implant position may correspond to early implant loosening and migration, and they differ from the reported literature.[19,22,23] Iannotti et al[8] studied the effect of implant design at liftoff as a surrogate for micromotion and implant fixation in foam block models. Their results showed superior fixation and less anterior glenoid liftoff for the step design with eccentric loading. They did test anterior-to-posterior eccentric loading, which provides the highest risk of loosening, but our results may vary because of variations in actual manufacturer implant design and kinematic loading conditions with abduction. It appears that not only loading conditions but also design variations are important considerations when examining implant fixation and micromotion, as Wahab et al[23] suggested that using an additional fifth peg will result in superior fixation stability to resist off-center loading compared with the two 4-peg designs whose results we examined. Further studies on micromotion must combine both loading conditions and critical implant design features to better understand outcomes and failure of augmented glenoid components.

This study should be interpreted in light of certain limitations. We used an average 50th percentile male subject as our joint model, which is not specific to or representative of all patients. In our FEA model, the cement mantle was modeled based on ideal conditions (1-mm thickness), which can be variable in clinical practice and may influence interpretation of our results. Our analysis simulated at least 5 years of implant wear performance with specific loading conditions and was isolated to evaluating micromotion; however, further studies would need to be performed to understand comparisons between these implants for long-term implant survival. This FEA isolated shoulder abduction modeling, whereas in a real-life situation, our prosthetic joint would be under the influence of multidirectional loading conditions, which were not accounted for in this study.

Conclusion

It is important to better understand the optimal augmented glenoid implant design through innovative FEA computer modeling that integrates physiological loading consistent with clinical outcomes and prediction of failures for TSA. On the basis of our FEA model, implant design slightly affects joint stability, whereas it plays a major role regarding implant fixation and long-term survival. Overall, an augmented wedge design provides better implant fixation and stress profiles with less micromotion. Further clinical studies are needed to validate these findings that will translate into better clinical outcomes and lower revision rates with selection of the optimal augmented implant design.

Disclaimer

This work has received an Orthopaedic Research and Education Foundation grant.

Vani J. Sabesan is a paid consultant for Arthrex and receives research support from Exactech. All the other authors, their immediate families, and any research foundations with which they are affiliated have not received any financial payments or other benefits from any commercial entity related to the subject of this article.

References

1. Allred JJ, Flores-Hernandez C, Hoenecke HR Jr, D'Lima DD. Posterior augmented glenoid implants require less bone removal and generate lower stresses: a finite element analysis. J Shoulder Elbow Surg 2016;25:823-30. http://dx.doi.org/10.1016/j.jse.2015.10.003
2. Anglin C, Wyss UP, Pichora DR. Mechanical testing of shoulder prostheses and recommendations for glenoid design. J Shoulder Elbow Surg 2000;9:323-31.
3. Boileau P, Sinnerton RJ, Chuinard C, Walch G. Arthroplasty of the shoulder. J Bone Joint Surg Br 2006;88:562-75. http://dx.doi.org/10.1302/0301-620x.88b5.16466

4. Cheung E V, Sperling JW, Cofield RH. Revision shoulder arthroplasty for glenoid component loosening. J Shoulder Elbow Surg 2008;17:371-5. http://dx.doi.org/10.1016/j.jse.2007.09.003
5. Day JS, Lau E, Ong KL, Williams GR, Ramsey ML, Kurtz SM. Prevalence and projections of total shoulder and elbow arthroplasty in the United States to 2015. J Shoulder Elbow Surg 2010;19:1115-20. http://dx.doi.org/10.1016/j.jse.2010.02.009
6. Hermida JC, Flores-Hernandez C, Hoenecke HR, D'Lima DD. Augmented wedge-shaped glenoid component for the correction of glenoid retroversion: a finite element analysis. J Shoulder Elbow Surg 2014;23:347-54. http://dx.doi.org/10.1016/j.jse.2013.06.008
7. Hopkins AR, Hansen UN, Amis AA, Taylor M, Emery RJ. Glenohumeral kinematics following total shoulder arthroplasty: a finite element investigation. J Orthop Res 2007;25:108-15. http://dx.doi.org/10.1002/jor.20290
8. Iannotti JP, Lappin KE, Klotz CL, Reber EW, Swope SW. Liftoff resistance of augmented glenoid components during cyclic fatigue loading in the posterior-superior direction. J Shoulder Elbow Surg 2013;22:1530-6. http://dx.doi.org/10.1016/j.jse.2013.01.018
9. Kersten AD, Flores-Hernandez C, Hoenecke HR, D'Lima DD. Posterior augmented glenoid designs preserve more bone in biconcave glenoids. J Shoulder Elbow Surg 2015;24:1135-41. http://dx.doi.org/10.1016/j.jse.2014.12.007
10. Knowles NK, Ferreira LM, Athwal GS. Premorbid retroversion is significantly greater in type B2 glenoids. J Shoulder Elbow Surg 2016;25:1064-8. http://dx.doi.org/10.1016/j.jse.2015.11.002
11. Langohr GD, Willing R, Medley JB, Athwal GS, Johnson JA. Contact mechanics of reverse total shoulder arthroplasty during abduction: the effect of neck-shaft angle, humeral cup depth, and glenosphere diameter. J Shoulder Elbow Surg 2016;25:589-97. http://dx.doi.org/10.1016/j.jse.2015.09.024
12. Mansat P, Briot J, Mansat M, Swider P. Evaluation of the glenoid implant survival using a biomechanical finite element analysis: influence of the implant design, bone properties, and loading location. J Shoulder Elbow Surg 2007;16(Suppl):S79-83. http://dx.doi.org/10.1016/j.jse.2005.11.010
13. Matsen FA 3rd, Clinton J, Lynch J, Bertelsen A, Richardson ML. Glenoid component failure in total shoulder arthroplasty. J Bone Joint Surg Am 2008;90:885-96. http://dx.doi.org/10.2106/JBJS.G.01263
14. Nguyen D, Ferreira LM, Brownhill JR, King GJ, Drosdowech DS, Faber KJ, et al. Improved accuracy of computer assisted glenoid implantation in total shoulder arthroplasty: an in-vitro randomized controlled trial. J Shoulder Elbow Surg 2009;18:907-14. http://dx.doi.org/10.1016/j.jse.2009.02.022
15. Nyffeler RW, Sheikh R, Atkinson TS, Jacob HA, Favre P, Gerber C. Effects of glenoid component version on humeral head displacement and joint reaction forces: an experimental study. J Shoulder Elbow Surg 2006;15:625-9. http://dx.doi.org/10.1016/j.jse.2005.09.016
16. Pomwenger W, Entacher K, Resch H, Schuller-Gotzburg P. Multi-patient finite element simulation of keeled versus pegged glenoid implant designs in shoulder arthroplasty. Med Biol Eng Comput 2015;53:781-90. http://dx.doi.org/10.1007/s11517-015-1286-7
17. Rice JC, Cowin SC, Bowman JA. On the dependence of the elasticity and strength of cancellous bone on apparent density. J Biomech 1988;21:155-68.
18. Rice RS, Sperling JW, Miletti J, Schleck C, Cofield RH. Augmented glenoid component for bone deficiency in shoulder arthroplasty. Clin Orthop Relat Res 2008;466:579-83. http://dx.doi.org/10.1007/s11999-007-0104-4
19. Sabesan VJ, Ackerman J, Sharma V, Baker KC, Kurdziel MD, Wiater JM. Glenohumeral mismatch affects micromotion of cemented glenoid components in total shoulder arthroplasty. J Shoulder Elbow Surg 2015;24:814-22. http://dx.doi.org/10.1016/j.jse.2014.10.004
20. Scalise JJ, Bryan J, Polster J, Brems JJ, Iannotti JP. Quantitative analysis of glenoid bone loss in osteoarthritis using three-dimensional computed tomography scans. J Shoulder Elbow Surg 2008;17:328-35. http://dx.doi.org/10.1016/j.jse.2007.07.013
21. Schwartz D, Guleyupoglu B, Koya B, Stitzel JD, Gayzik FS. Development of a computationally efficient full human body finite element model. Traffic Inj Prev 2015;16(Suppl 1):S49-56. http://dx.doi.org/10.1080/15389588.2015.1021418
22. Sukjamsri C, Geraldes DM, Gregory T, Ahmed F, Hollis D, Schenk S, et al. Digital volume correlation and micro-CT: an in-vitro technique for measuring full-field interface micromotion around polyethylene implants. J Biomech 2015;48:3447-54. http://dx.doi.org/10.1016/j.jbiomech.2015.05.024
23. Wahab AH, Kadir MR, Harun MN, Kamarul T, Syahrom A. Number of pegs influence focal stress distributions and micromotion in glenoid implants: a finite element study. Med Biol Eng Comput 2017;55:439-47. http://dx.doi.org/10.1007/s11517-016-1525-6
24. Walch G, Badet R, Boulahia A, Khoury A. Morphologic study of the glenoid in primary glenohumeral osteoarthritis. J Arthroplasty 1999;14:756-60.
25. Walch G, Boulahia A, Boileau P, Kempf JF. Primary glenohumeral osteoarthritis: clinical and radiographic classification. The Aequalis Group. Acta Orthop Belg 1998;64(Suppl 2):46-52.
26. Wang VM, Krishnan R, Ugwonali OF, Flatow EL, Bigliani LU, Ateshian GA. Biomechanical evaluation of a novel glenoid design in total shoulder arthroplasty. J Shoulder Elbow Surg 2005;14(Suppl S):129S-140S. http://dx.doi.org/10.1016/j.jse.2004.09.029
27. Wirth MA, Rockwood CA Jr. Complications of total shoulder-replacement arthroplasty. J Bone Joint Surg Am 1996;78:603-16.
28. Yongpravat C, Kim HM, Gardner TR, Bigliani LU, Levine WN, Ahmad CS. Glenoid implant orientation and cement failure in total shoulder arthroplasty: a finite element analysis. J Shoulder Elbow Surg 2013;22:940-7. http://dx.doi.org/10.1016/j.jse.2012.09.007
29. Zhang J, Yongpravat C, Kim HM, Levine WN, Bigliani LU, Gardner TR, et al. Glenoid articular conformity affects stress distributions in total shoulder arthroplasty. J Shoulder Elbow Surg 2013;22:350-6. http://dx.doi.org/10.1016/j.jse.2012.08.025
30. Zumstein V, Kraljevic M, Hoechel S, Conzen A, Nowakowski AM, Muller-Gerbl M. The glenohumeral joint—a mismatching system? A morphological analysis of the cartilaginous and osseous curvature of the humeral head and the glenoid cavity. J Orthop Surg Res 2014;9:34. http://dx.doi.org/10.1186/1749-799X-9-34